Electronic Supplementary Information

A novel hybrid triboelectric nanogenerator based on the mutual boosting effect of electrostatic induction and electrostatic breakdown

*Ai Chen,‡ Qixuan Zeng,‡ Liming Tan, Fan Xu, Tingyu Wang, Xiaofang Zhang, Yanlin Luo, Xue Wang**

Department of Applied Physics, Chongqing University, Chongqing 400044, P. R. China

** E-mail: xuewang@cqu.edu.cn (X Wang)*

† Electronic Supplementary Information (ESI) available: [details of any supplementary information available should be included here]. See DOI: 10.1039/x0xx00000x

‡ These authors contributed equally to this work.

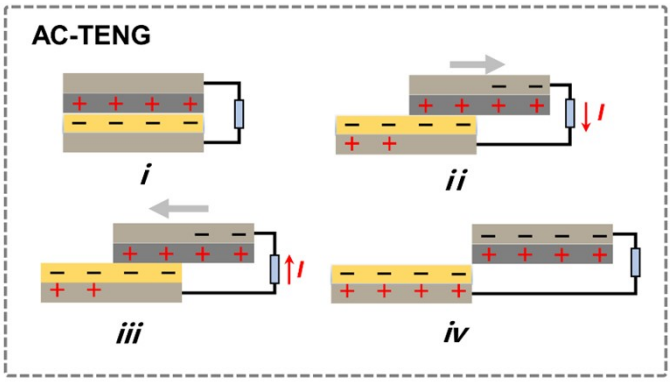

Fig. S1 Working mechanism of the AC-TENG.

Note S1. Working mechanism of S-TENG based on the coupling of triboelectrification and electrostatic induction.

The AC-TENG consists of a top induction electrode (covered on PU) on its slider and a bottom induction electrode (covered on PTFE film) on its stator part. The working mechanism of the device is displayed in **Fig. S1**. Because of charge transfer between PU and PTFE surfaces with different surface electron affinity, there are positive charges on the PU surface and equivalent opposite charges on the PTFE surface. When an external force is applied to the slider, the periodic change in the overlapped area between electrodes causes the periodic change in the potential difference between the electrodes through electrostatic induction, thus generating an alternating current (AC) output in the external circuit to balance the potential difference.

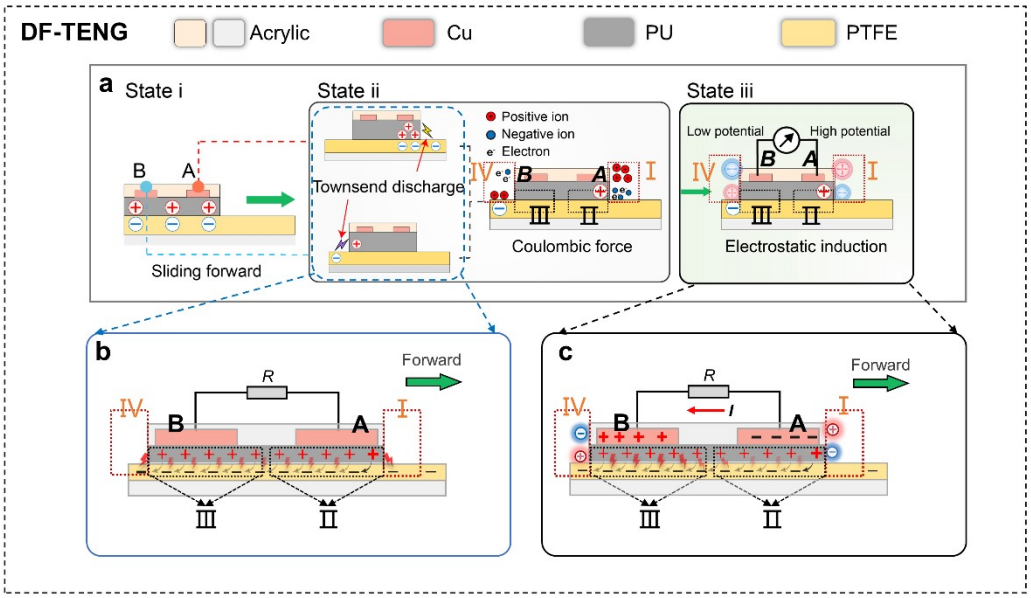

Fig. S2 Working mechanism of the DF-TENG. (a) Working mechanism of DF-TENG, including three states: State (i) triboelectrification, State (ii) electrostatic breakdown, Stage (iii) electrostatic induction; the States (ii) and (iii) mainly demonstrate the charge distribution at the two ends of the slider. (b) Enlarged interface states of State (ii). (c) Enlarged interface state of State (iii); due to the continuous current from electrode A to B, there is an electrostatic breakdown suppression area II below electrode A and electrostatic breakdown enhancement area III below electrode B.

Note S2. Working mechanism of DF-TENG based on the convergence of triboelectrification, electrostatic induction, and electrostatic breakdown.

The DF-TENG primarily consists of a slider and a stator, as shown in **Fig. S2**. To be specific, a polytetrafluoroethylene (PTFE) film is attached onto the surface of an acrylic plate as the stator, while a pair of copper (Cu) electrodes is arranged at the back of the polyurethane (PU) slider, completely covered by an insulating layer

(acrylic sheet). In order to describe the working principle of DF-TENG, only one moving direction is taken as an example. We labeled the electrodes as Electrodes A and B, and they are respectively located at the front and rear ends of the slider. At the initial state (**State i in Fig. S2a**), the motion direction of the PU slider is assumed to be forward, and the two electrodes will be in different states due to their spatial position difference. According to triboelectrification, the surface of PU and PTFE film will be positively and negatively charged. At **State ii**, the PU block keeps moving forward, and a large number of electrostatic breakdowns occur at the friction interface due to the PU with many evenly distributed open micropores (pore diameter ~10-100 μm) on its surface. This process leads to the surface charges re-releasing, facilitating the next-step triboelectrification (**Fig. S2b**). Therefore, the incorporation of triboelectrification and electrostatic breakdown at the frictional interface facilitates transferring charges between the dielectric layers. From a microscopic view, electrostatic discharge always lags behind triboelectrification. After the electrostatic breakdown, the tribo-charges cannot be completely released, and some residual charges remain on the tribo-layer surfaces. Thus, for the PTFE behind the slider, the net charge is negative. And for the front area of the PU block, the net charge is positive, since it will be continuously tribo-charged because the PTFE surface in front of the PU slider is unsaturated. According to Townsend's discharge theory, along with the discharge process, a large number of charged particles are produced in the air, including positive ions, negative ions, and electrons (**State ii, Fig. S2a**). After that, due to the interaction of coulomb force between net charges and charged particles, the

positive and negative air ions will be electrostatically repelled and move close to Electrode A and B, respectively. Therefore, an electric potential difference will be built between the two electrodes, and a constant current output from electrode A into B will be generated via electrostatic induction (**State iii, Fig. S2a, and Fig. S2c**). Once the slider comes into a moving backward, an opposite output will be produced. As a result, the DF-TENG can generate AC/DC convertible output by changing motion states.

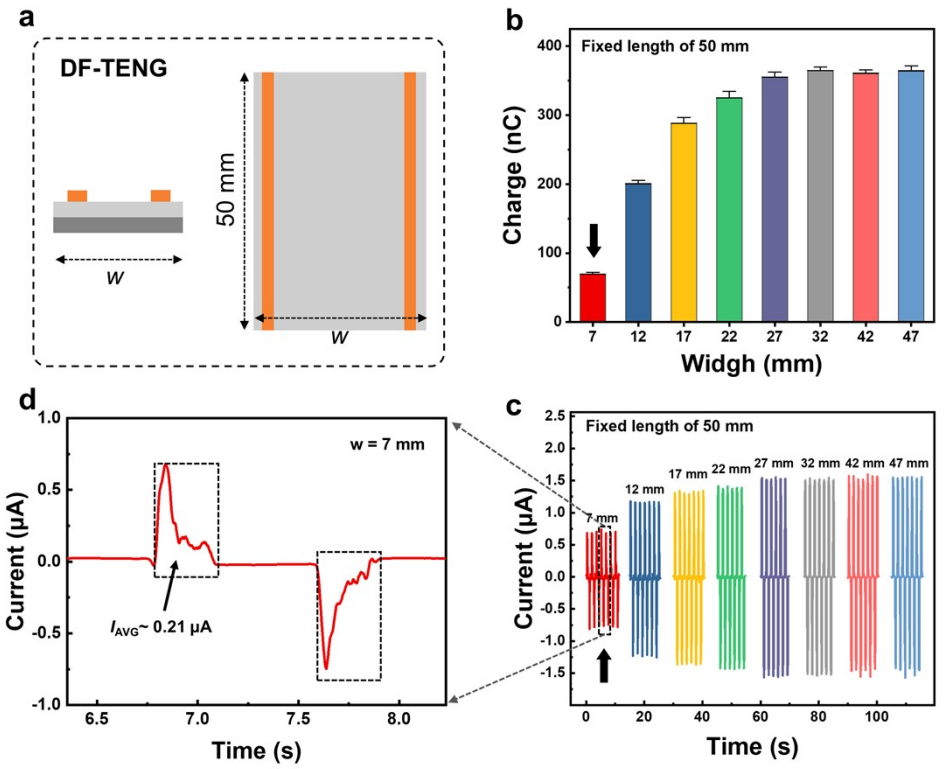

Fig. S3 The electrical output of H-TENG (electrodes are located at both ends of the slider) under different slider widths at 0.1 m s^{-1} (fixed length of 50 mm). (a) Schematic of dimensions of DF-TENG. (b) transfer charge. (c) Short-circuit current. (d) Enlarged view of the short-circuit current while the width of 7 mm.

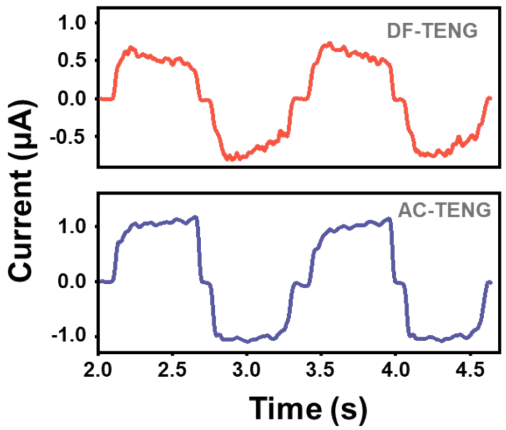

Fig. S4 Output current curves of H-TENG in two working cycles.

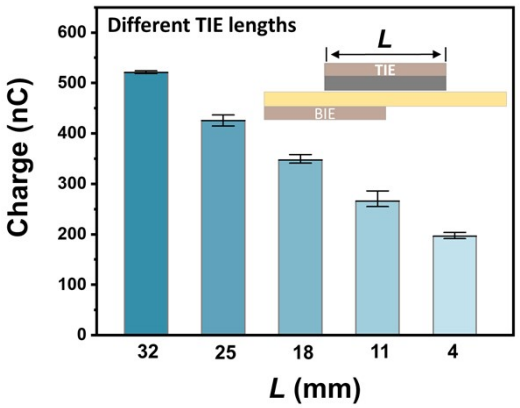

Fig. S5 Transfer charge of AC-TENG with various TIE lengths. It is worth noting that, in the H-TENG, the transferred charge of the AC part reaches up to 518.8 nC, which is 21.7% higher than that of the sole AC device with the same TIE length of 25 mm and even close to that of the device with electrode TIE length of 32 mm.

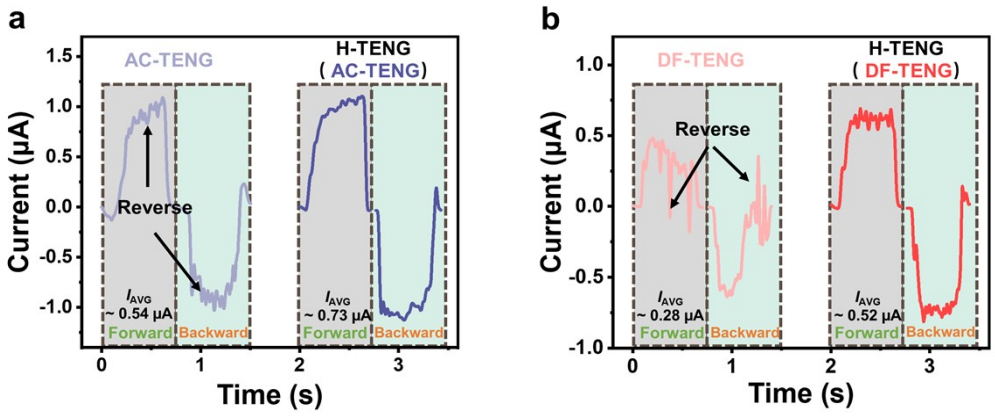

Fig. S6 Current output comparisons of H-TENG with the sole AC-TENG and DF-TENG. (a) The output currents of AC-TENG within H-TENG and the sole AC-TENG, reflecting the effect of the DF-TENG on the output of AC-TENG. (b) The output current of DF-TENG within H-TENG and the sole DF-TENG, demonstrating the influence of the AC-TENG on the output of DF-TENG.

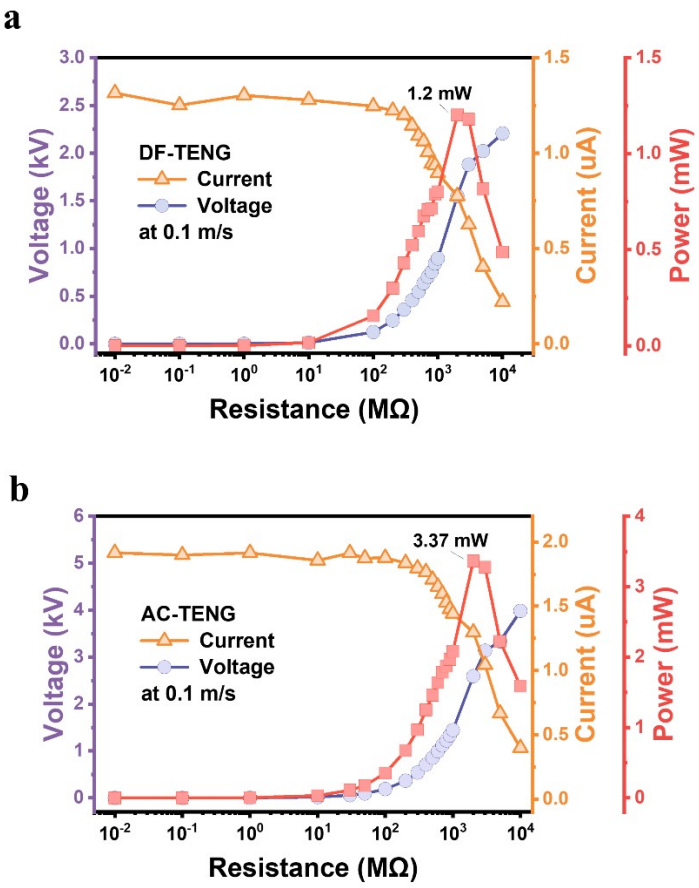

Fig. S7 Output current, voltage, and power of DF-TENG (**a**) and AC-TENG (**b**) when sliding mode H-TENG is in reciprocating condition.

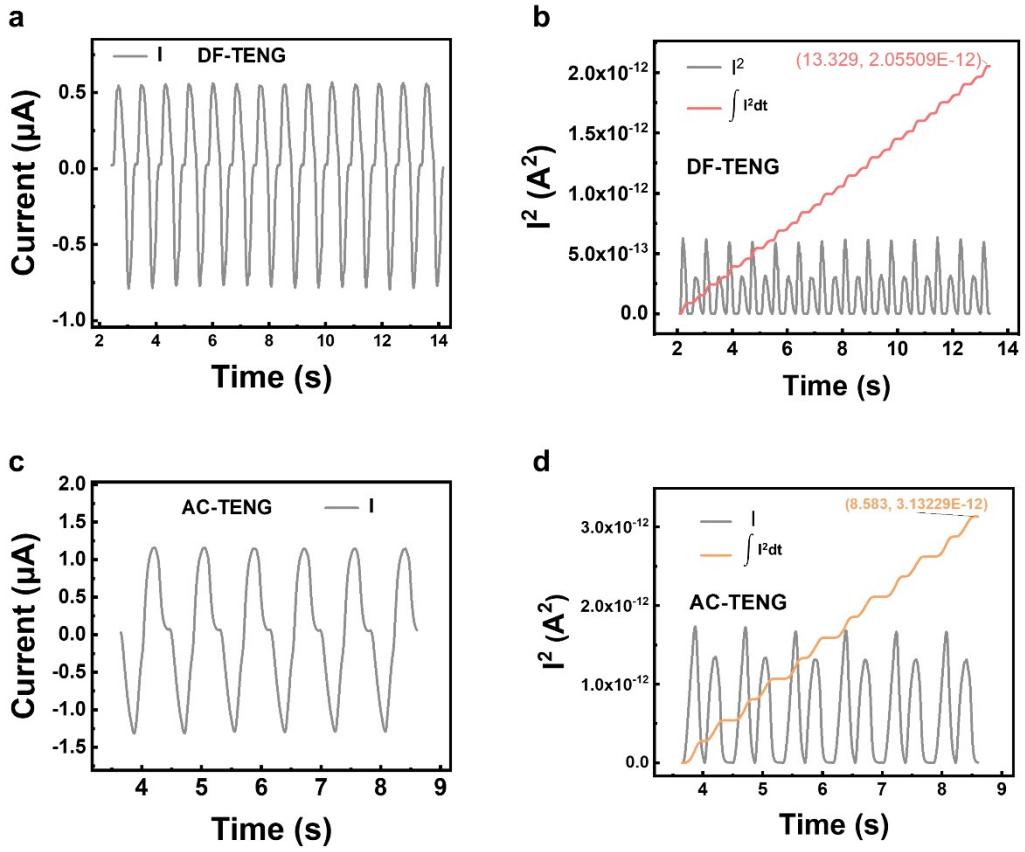

Fig. S8 (a) I and (b) I^2(corresponding integrating curve in red) of DF-TENG with 2 GΩ load in sliding mode H-TENG. (c) I and (d) I^2 (corresponding integrating curve in orange) of AC-TENG with 2 GΩ load in sliding mode H-TENG.

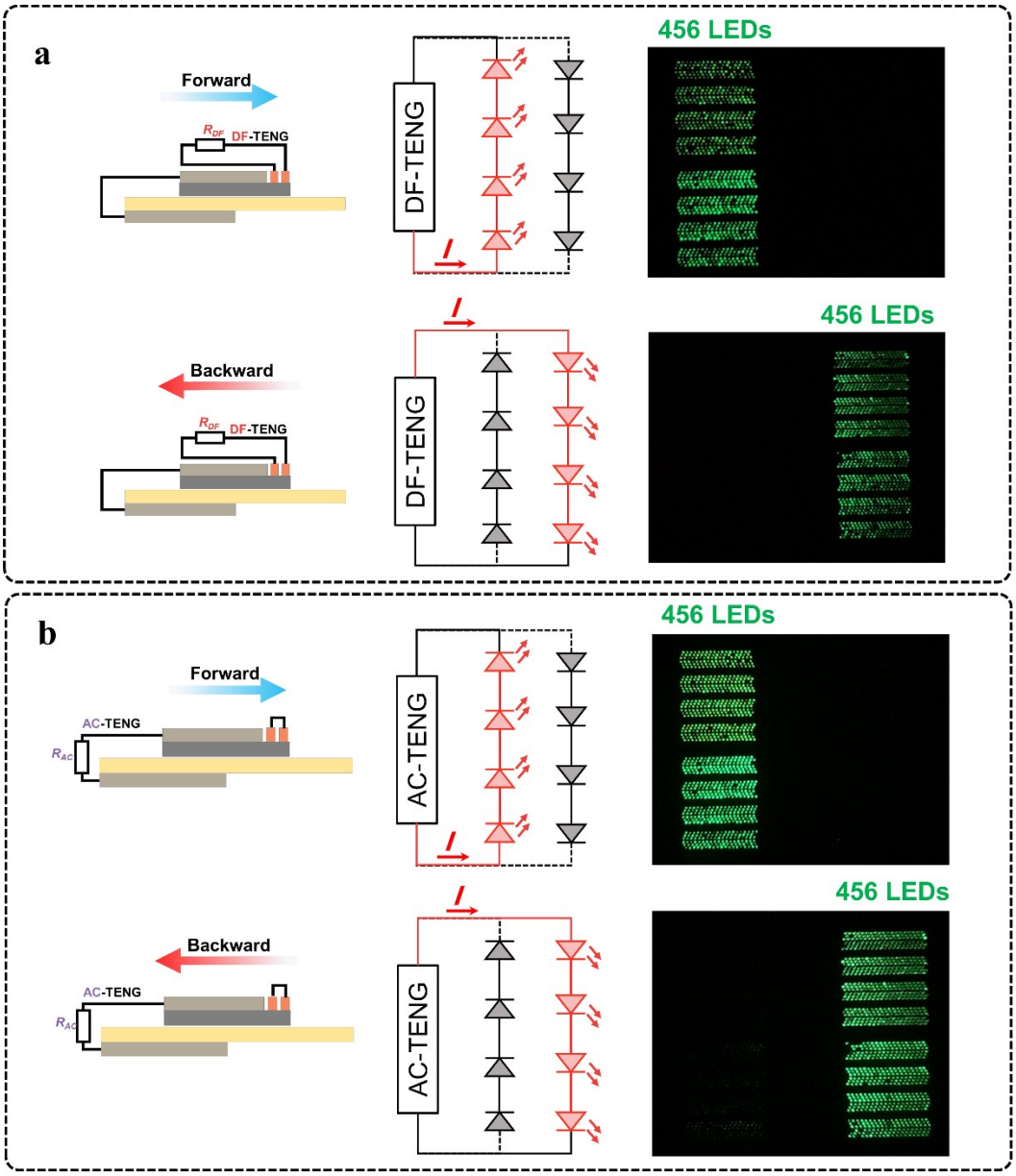

Fig. S9 Two LED arrays (each one consisting of 456 LEDs connected in series) are alternately driven by DF-TENG (**a**) or AC-TENG (**b**) within sliding mode H-TENG.

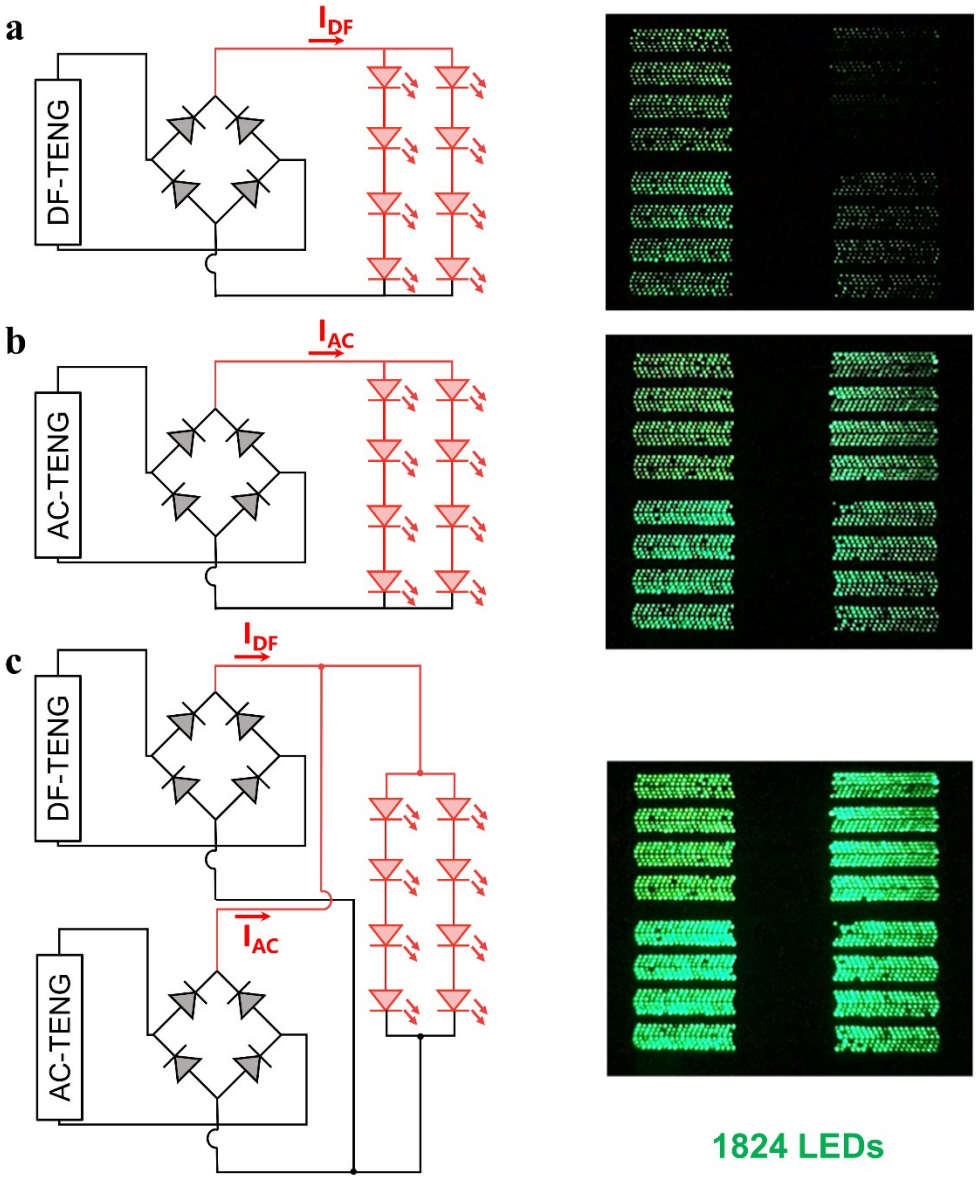

Fig. S10 An 1824 LEDs array driven by DF-TENG (a), AC-TENG (b), or integrated output (c) within sliding mode H-TENG.

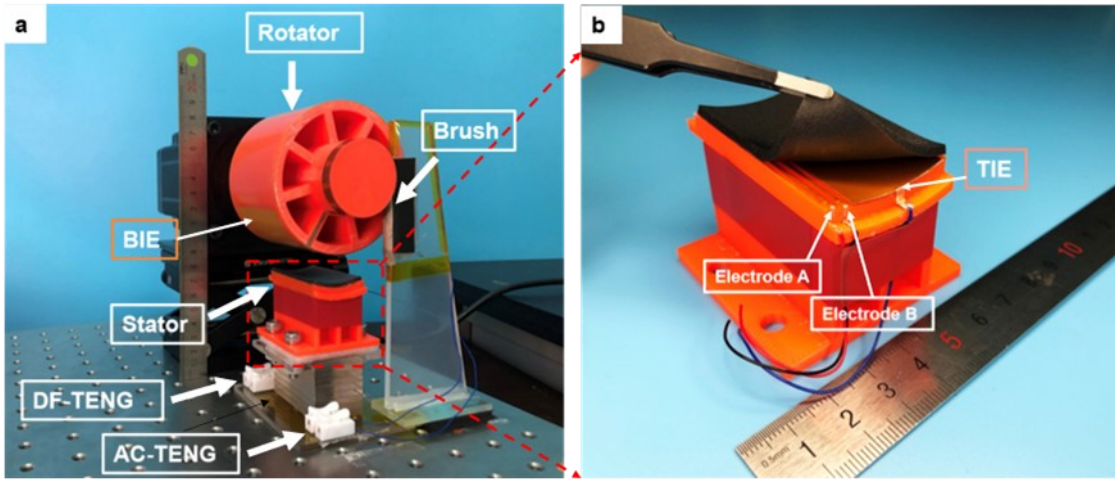

Fig. S11 Physical photos of rotary mode H-TENG (a) and enlarged view of its stator (b).

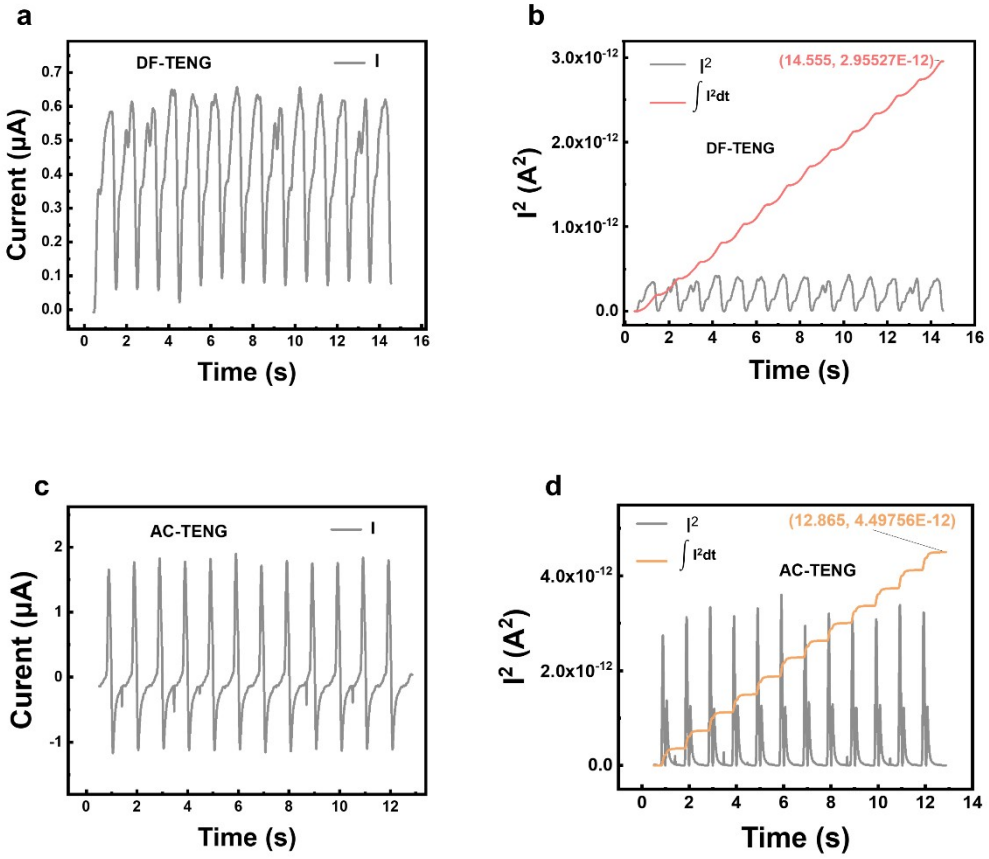

Fig. S12. (a) I and (b) I^2 (corresponding integrating curve in red) of DF-TENG with 5 GΩ load for rotary H-TENG; (c) I and (d) I^2 (corresponding integrating curve in orange) of AC-TENG with 1 GΩ load for rotary mode H-TENG.

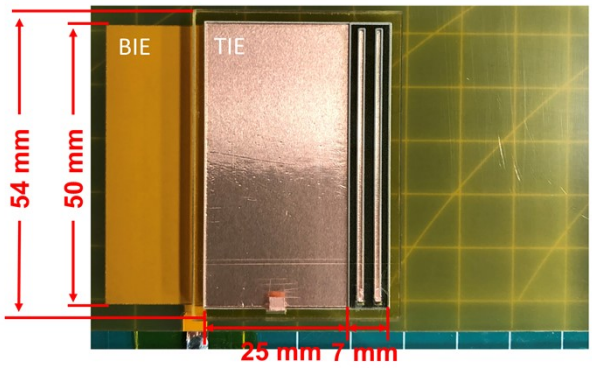

Fig. S13 The detailed dimensions of sliding mode H-TENG

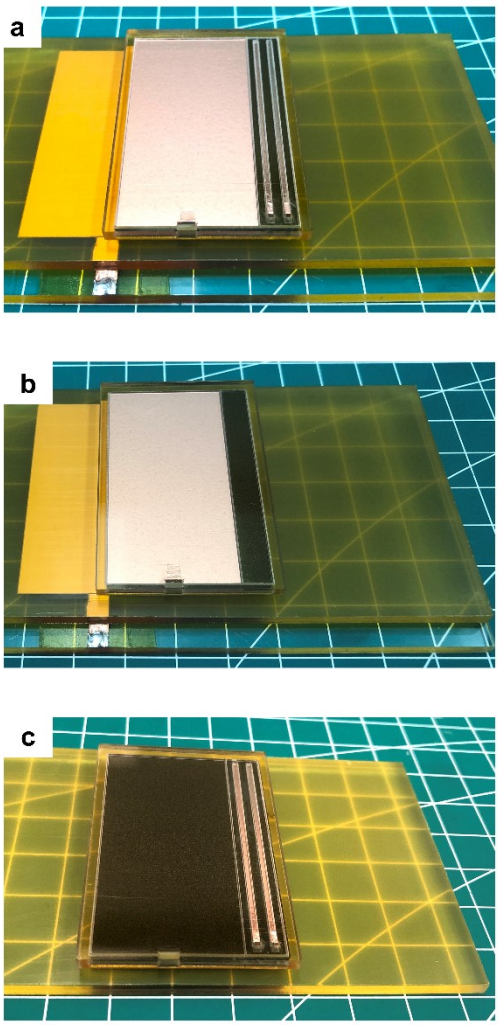

Fig. S14 Physical photographs of discrete devices: H-TENG (a), AC-TENG (b), and DF-TENG (c).

Note S3. The calculation process of average power density based on H-TENG.

According to Equation 1, the average power density is calculated by Origin Lab and the relevant calculation.

$$P_{Average} = \frac{\int_{t_1}^{t_2} I^2 dt}{\Delta t} \quad (1)$$

As for sliding mode H-TENG, **Figs. S8a and c** present the current value at matched impedance (2 GΩ), and **Figs. S8b and d** represent the curve of I^2. According to Equation (1), then integrate I^2 over time, represented by a red line **in Figs. S8b and d**. The same process is performed for rotary mode H-TENG, as shown in **Fig. S12**. **Tables S1 and S2** show the various parameter values in the actual calculation process.

Table S1. Relevant data for calculating the P_{APD} of sliding mode H-TENG with dual AC outputs

	A	B	C	D	E	F	G	I
	t_1	t_2	$\int_{t_1}^{t_2} I^2 dt$	Δt	C/D	ER (Average power)	f (Hz)	Average power density at 1Hz
DF-TENG	2.91 s	14.16 s	2.06E-12	11.24	1.83E-13	0.37 mW	1.56	0.68 W·m^{-2}
AC-TENG	3.64 s	8.60 s	3.13E-12	4.96	6.31E-13	1.26 mW	1.56	0.65 W·m^{-2}
H-TENG	Total average power density output						1.56	1.33 W·m^{-2}

Table S2. Relevant data for calculating the P_{APD} of rotary mode H-TENG with AC and DC outputs

	A	B	C	D	E	F	G	H
	t_1	t_2	$\int_{t_1}^{t_2} I^2 dt$	Δt	C/D	ER (Average power)	f (Hz)	Average power density at 1Hz
DF-TENG	0.43 s	14.56 s	2.96E-12	14.13	2.09E-13	1.05 mW	1	3.00 W·m^{-2}
AC-TENG	0.51 s	12.87 s	4.50E-12	12.36	3.64E-13	0.36 mW	1	0.29 W·m^{-2}
H-TENG	Total average power density output						1	3.29 W·m^{-2}

Other Supplementary Material for this work includes the following:

Video S1. Two LED arrays (each one 456 LEDs) were alternatively driven by DF-TENG or AC-TENG within sliding mode H-TENG.

Video S2. A LED array (1824 LEDs) was driven by the integrated output, AC-TENG, or DF-TENG within sliding mode H-TENG.

Video S3. Two LED arrays (each one 456 LEDs) are driven by DF-TENG or AC-TENG within rotary mode H-TENG.

Video S4. A LED array (1824 LEDs) is driven by rotary mode H-TENG (integrated output) at 120 rpm.

Video S5. A commercial calculator was powered by H-TENG at 120 rpm.